

SURFACE PRESSURE VARIATION ON AN AIRFOIL IN PLUNGING AND PITCHING MOTIONS

M.R. Soltani, F. Rasi Marzabadi and M. Seddighi
Sharif University of Technology, Tehran, Iran

Keywords: *Plunging- Pitching- unsteady- wind tunnel- reduced frequency.*

Abstract

Unsteady aerodynamic experiments were conducted on an oscillating airfoil in a subsonic wind tunnel. The model was oscillated in two types of motion, pitch and plunge, at a range of reduced frequencies, $k=0.029-0.1$. In addition, steady data were acquired and examined to furnish a baseline for analysis and comparison. The unsteady surface pressure is measured along the chord for both upper and lower surfaces of the model. Particular emphases were placed on the effects of different types of motion on the unsteady pressure distribution of the airfoil at pre-stall, near stall, and post stall conditions. It was found that the variations of the pressure distribution with angle of attack have strong sensitivity to the displacement, oscillating frequency and mean angles of attack. The width of the hysteresis loop, position of the “figure 8 shape” and slope of the pressure coefficient curve have been influenced by both types of motion, pitch and plunge.

Nomenclatures

- α Angle of attack
- h Plunging displacement
- \bar{h} Dimensionless plunging amplitude
- $\bar{\alpha}$ Amplitude of the pitching motion (deg)
- k Reduced frequency, $k = \frac{\pi f c}{U_\infty}$
- f Oscillation frequency (Hz)
- U_∞ Free stream velocity
- c Airfoil chord (m)
- τ Dimensionless time, $\tau = t / T$
- α_0 Mean incidence angle (deg)

- C_p Pressure coefficient
- L.E. Leading edge
- T.E. Trailing edge
- $()_{eq}$ Equivalent motion

1 Introduction

Unsteady flows over lifting surfaces occur in a wide range of new and old aerodynamic vehicles. A few examples of such devices are such as turbo machines, high-performance aircraft, helicopter rotors, and wind turbine blades, which have received considerable attentions in recent years due to the generation of electrical power [1 -3].

The unsteady flows around the airfoil are rather complicated. Unsteady pressure fluctuations on the airfoil produce vibrations and radiate noise. Because of their complicated, rapidly changing time depended nature, significant amount of research both theoretical and experimental has been conducted to understand the fluid mechanics of flow fields around an airfoil oscillating in pitch [4-8].

Wind turbines operate for most of their time in an unsteady flow environment [9, 10]. The airloads on each blade element vary in time because the turbine is usually yawed with respect to the oncoming wind and further because of shear in the ambient wind, ambient turbulence, blade flapping and vibratory displacements, etc. Unsteady effects associated with wind turbines are particularly acute because of large perturbations and the corresponding high effective reduced frequencies. These phenomena contribute

significantly to the unsteady flow environment on the blades [1].

The analysis of Horizontal Axis Wind Turbine (HAWT) blade loads is subdivided into two major areas: dynamic stall and dynamic inflow [11]. McCroskey [12] presents an excellent review of dynamic stall phenomenon. All wind turbines operate with some parts of the blade stalled for a portion of the time. Prior to 1988 dynamic stall and unsteady aerodynamic effects were not included in HAWT performance and load analysis. In 1988 Butterfield was able to quantify both the existence dynamic stall and its effect on rotor loads by measuring pressure distributions on a 10m HAWT [11].

This paper examines the effect of pitching and plunging displacements on unsteady airfoil behavior. A one-to-one correspondence was established between pairs of pitching and plunging motions according to the potential flow transformation formula. The imposed variables of the experiment were reduced frequency, mean angle of attack and amplitude of motion.

2 Experimental Apparatus

The experiments were conducted in the low speed wind tunnel in Iran. It is a closed circuit tunnel with rectangular test section of $80 \times 80 \times 200 \text{ cm}^3$ and has a total dimension of $3.8 \times 6.5 \times 18 \text{ m}^3$. The test section speed varies continuously from 10 to 100 m/sec, at Reynolds number of up to 5.26×10^6 per meter. The model considered in the present study has 25cm chord and 80cm span which is the model of a 660 kW wind turbine blade section. This airfoil is equipped with 64 pressure orifices on the upper and lower surfaces. The pressure ports are located along the chord at angle of attack of 20 degrees with respect to the model span to minimize disturbances from the upstream taps, Fig. 1. Data were obtained using sensitive pressure transducers. Due to high number of pressure ports and the size of the selected pressure transducers, it wasn't possible to place the transducers inside the model. Therefore,

extensive experiments were conducted to ensure that the time takes for the pressure to reach the transducers is much less than the frequency response of the transducers themselves [13]. Finally the tube length and material that gave minimum time lag for all applied pressures was selected. Each transducer data is collected via a terminal board and transformed to the computer through a 64 channel, 12-bit Analog-to-Digital (A/D) board capable of an acquisition rate of up to 500 kHz. The oscillation system for the plunging motion uses a crankshaft to convert the circular motion of the motor to a reciprocal motion, which is transferred to the model by means of a rod. The pitch rotation point is fixed about the wing quarter chord. The model angle of attack was varied sinusoidally as $\alpha = \alpha_0 + \sin(\omega t)$. These two systems can oscillate the model at various amplitudes, mean angles of attack, and frequencies ranging from 1 to 4 Hz. Fig. 2 shows the oscillating mechanism used in this investigation.

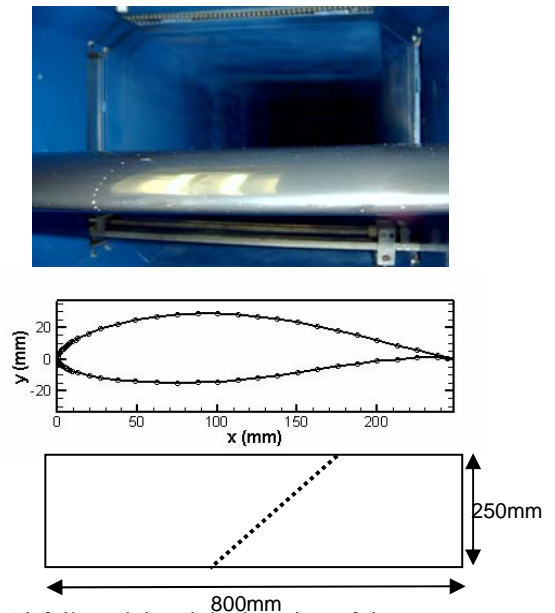


Fig. 1. Airfoil model and the location of the pressure ports

Dynamic oscillatory data presented here are an average of several cycles at a sample rate based on the oscillation frequency. Various data acquisition rates were examined to find the best combination, which would provide as many cycles of quality data as possible. Raw data were then digitally filtered using a low-pass

SURFACE PRESSURE VARIATION ON AN AIRFOIL IN PLUNGING AND PITCHING MOTIONS

filtering routine. During the filtering process, cut off and transition frequencies were varied until the deviation between the original and the filtered data was a minimum. Finally, all dynamic data were corrected for the solid tunnel sidewalls and the wake blockage effects using the method explained in Ref. [15] for the static data. For the dynamic case, the model was oscillating and the data for all ports were collected when the tunnel was off. The oscillation frequency as well as the acquisition constants was exactly equal to those during tunnel on conditions. All pressure data acquired during the tunnel on condition were subtracted from those obtained during tunnel off situation to account for the inertial effects.



a) Pitching system



b) Plunging system

Fig. 2. Pitching and plunging oscillation systems

3 Results and Discussion

An extensive experimental investigation was conducted on an oscillating airfoil in two different modes, pitching and plunging, over a range of reduced frequencies, $k=0.029-0.1$ and various oscillation amplitudes. The airfoil surface pressure distribution was measured at

velocity of 30 m/sec, corresponding to the Reynolds number of $0.42 \cdot 10^6$. The static angles were varied from -5 to 25 degrees.

The plunging displacements were transformed into equivalent angles of attack using the potential flow transformation formula, $\bar{\alpha}_{eq} = ik\bar{h}$, where $\bar{\alpha}_{eq}$ is in radians and \bar{h} has been nondimensionalized with respect to the model semi-chord. The mean angle of attack was, of course, added to the equivalent angle [12, 14].

The motion of the plunging airfoil varies sinusoidally with time, hence the corresponding induced angle of attack, which is due to the oscillation time history effects on the vertical motion of the model, is 90 degrees out of phase. Also the motion of the pitching airfoil varies sinusoidally with time. Fig. 3 shows an example for the variation of the equivalent angle of attack for one oscillation cycle with respect to its corresponding time history of the plunging motion and the real variation of the angle of attack with time in a pitching motion. It can be seen that α_{eq} is a maximum or a minimum whenever $h=0$ during upstroke or down stroke motions, respectively.

Figures 4 and 5 compare the pressure coefficient variations with dimensionless time and the corresponding angle of attack for motions, pitching and plunging, for several pressure ports, both upper and lower surfaces. The model was set to an angle of 5 degrees and oscillated at reduced frequencies of $k=0.029$ and 0.087 . Selected pressure ports are located at $x/c=5\%$ and 50% , before and after the maximum thickness of the airfoil which is at about $x/c=35\%$, respectively. Shown in the C_p - α graph is the direction of the hysteresis loops too.

From figure 4a and 4b, it is seen that for the upper surface pressure ports, the variation of the pressure coefficients with dimensionless time is nearly the same as the variations of the angle of attack with time for both types of motion similar to that of fig. 3b. From this figure it is seen clearly that for these ranges of angles of attack, the flow is attached during the entire cycle. However, absolute value of C_p varies from each other, i.e. $|C_{pmax}|$ for the

pressure port located at $x/c=5\%$ is higher than that of $x/c=50\%$. Furthermore by inspecting variation of C_p versus τ , it is clearly seen that $|C_{pmax}|$ for the pressure ports located at $x/c=5\%$ of the upper surface both for pitching and plunging motions, does not occur when α has its maximum value.

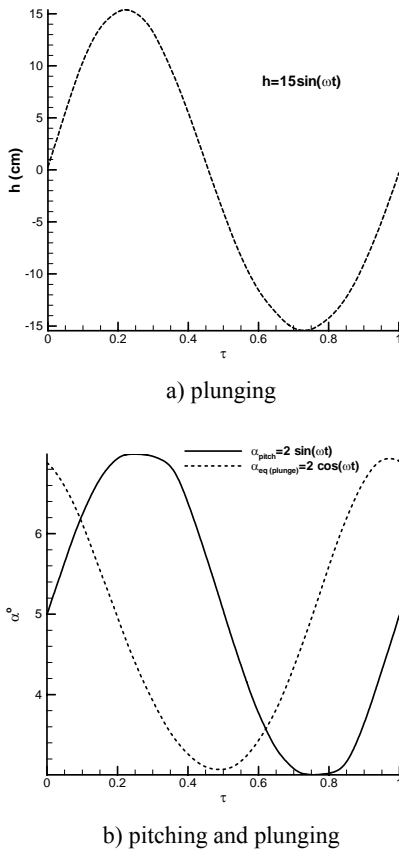


Fig. 3. Time history of the pitching and plunging motion with its corresponding equivalent angle of attack

Figure 6a shows that for the pitching motion, $|C_{pmax}|$ occurs at $\tau \approx 0.31$, while it takes about, $\tau=0.25$, for the model to reach its maximum angle of attack. It is further seen that by increasing the reduced frequency to $k=0.087$, $|C_{pmax}|$ occurs at a later time, $\tau \approx 0.43$, figure 5a. This phenomenon is also seen for the plunging motion. The maximum equivalent angle of attack is at $\tau=0$, but $|C_{pmax}|$ does not occur at this time and for $k=0.029$, it occurs at $\tau \approx 0.05$ while for $k=0.087$, $|C_{pmax}|$ occurs at $\tau \approx 0.18$. Also it is noted that the phase difference of 90 degrees, or $\Delta\tau=0.25$ between pitching and plunging angles of attack, is not affected by the reduced

frequency and the effect of k on the pressure-gradient-lag is the same for both types of motions.

By inspecting the C_p - α graphs, it is seen that for $k=0.029$ the width of the hysteresis loop is nearly the same at pressure port located at $x/c=5\%$ for both pitching and plunging motions; but for the pressure ports located at the $x/c=50\%$ and of the lower surface, the hysteresis loop is wider for the plunging case and this difference become larger toward the trailing edge, figures 4d and 4c. Also for the higher reduced frequency case, $k=0.087$, the width of the hysteresis loops increases for the lower surface pressure ports and this increase is more for the plunging motion, figures 5d and 5c. The pressure response actually has contributions from both angles of attack and pitch-rate terms. This difference between two types of motion is due to the present of the pitch-rate in the pitching oscillation which is absent in the plunging case.

By inspecting the direction of the C_p - α hysteresis loops, it is seen that for the upper surface pressure ports, the directions are counterclockwise that means the flow in the upstroke motion lags that of the down stroke one. While, for the pressure ports located at the lower surface, the situation is reversed. Furthermore, note that for both pitching and plunging oscillations, by increasing the reduced frequency, the suction peak and hence the mean slope of the C_p - α graph especially for the pressure port located near the leading edge, reduces too. This indication is because of the effect of the shed wake that increases at higher reduced frequencies.

Figures 6 and 7 show variations of the surface pressure with angle of attack for the same pressure ports, $x/c=5\%$ and 50% , when the model is set to mean angle of attack of 10 degrees. For this airfoil, static stall angle of attack is about 10 degrees. Oscillating the airfoil in this region, results in an unsteady airfoil stall or dynamic stall behavior. This is characterized by two distinctly different flow phenomena: the delay of stall due to the time lag and boundary layer improvement effects, which is quasi-steady in nature, and the transient behavior of

SURFACE PRESSURE VARIATION ON AN AIRFOIL IN PLUNGING AND PITCHING MOTIONS

the formation and "spillage" of a leading-edge or dynamic vortex. The pressure-gradient-lag effect is the same for both pitching and plunging cases. However, the "leading-edge jet" effects are of opposite kinds, delaying separation phenomenon for the pitching and promoting it for the plunging airfoil. By inspecting these figures it is seen that for the upper surface pressure ports, especially for the ports behind the location of maximum thickness, $x/c=35\%$, the width of the hysteresis loop of C_p in the pitching motion with respect to the plunging case, decreases drastically. As the reduced frequency is increased from $k=0.029$ to $k=0.087$, the width of the hysteresis loops is increased for the pitching airfoil, however, for plunging airfoil the opposite is true. Furthermore, the direction of the hysteresis loops for the upper surface ports has been changed too. Figures 8 and 9 show dynamic variations of the pressure coefficient with angle of attack for pressure ports located at $x/c=2\%$ and 5% of the upper and lower surfaces, at reduced frequencies of $k=0.029$ and 0.087 , for both pitching and plunging oscillations. The model was set to a mean angle of attack of 18 degrees. In this case the variations of the C_p have nearly the same trends for both pitching and plunging motions. The direction of the hysteresis loops is clockwise for the upper surface pressure ports indicating that the flow over these pressure ports in the upstroke motion leads that of the down stroke one. While for the pressure ports located at the lower surface, the reverse is true. For the pressure port located at $x/c=2\%$, there is no effect of flow separation, but at $x/c=5\%$ and for $k=0.029$, it is seen that the pressure coefficient increases as the angle of attack increases and then drops sharply by further increasing the angle of attack. For the pitching motion at an angle of attack of about 17.5 degrees, $|C_p|$ drops sharply while for the plunging motion, the separation is seen at an angle of attack of about 16.5 degrees. The delay in separation for the pitching airfoil is due to the effect of pitch-rate and the leading-edge jet effect, figure 8. For the higher value of reduced frequency case, $k=0.087$, it is seen that the width of the hysteresis loop for the pitching case

increases compared to that of $k=0.029$ for all pressure ports. In contrast, for the plunging motion, this trend is reversed.

Fig. 10 shows the carpet plot of C_p distribution for three different mean angles of attack. The comparison is done to investigate the effect of mean angle of attack on two different types of motion, for $\alpha_0=5^\circ$, 10° and 18° .

By inspecting figures 10a to 10c, it is seen that by oscillating the airfoil at higher mean angles of attack, the maximum suction, $|C_{p_{max}}|$, increases and its location moves toward the leading edge. It is further seen that $|C_{p_{max}}|$ is about 1.4 for both pitching and plunging motions, and its location is near $x/c=18\%$, Fig. 10a. In this case as seen from Fig. 10a, the pressure ports located at $0 < x/c < 40\%$, carry maximum loads. For $\alpha_0=10^\circ$, $|C_{p_{max}}| \approx 3.2$ and occurs at about $x/c=0.5\%$, Fig. 10b while for $\alpha_0=18^\circ$, $|C_{p_{max}}| \approx 4.8$ and its location is very close to the leading edge, Fig. 10c. Furthermore, from Fig. 10c it is evident that $|C_{p_{max}}|$ drops sharply and is followed by a constant pressure region from $x/c > 0.5\%$. This indicates that for this mean angle of attack case, the flow has been separated over an extensive area of the airfoil upper surface.

Figures 11 and 12 show the effect of oscillating amplitude for pitching and plunging motions, at $\alpha_0=5$ and 18 degrees, respectively. The variations of C_p with dimensionless time and angle of attack for the pressure ports located at $x/c=5\%$ of the upper and lower surfaces are shown. By inspecting these figures, it is clearly seen that the effect of oscillation amplitude for both pitching and plunging oscillations is the same as the effect of reduced frequency and it increases unsteadiness of the flow, hence widening the hysteresis loops. From C_p - τ figures, it is seen that as the oscillation amplitude increases, the variation of the pressure coefficient become similar to the time history of each motion, pitching and plunging. Also it is seen that contrary to the pitching motion, for the plunging airfoil the slope of the C_p - α curve for the upper surface pressure ports, increases with increasing the oscillation amplitude. When the model was set to mean angle of attack of 18 degrees, figure 12, from

C_p - τ graphs it is seen that for both pitching and plunging motions, $|C_p|$ starts to decrease at $\tau=0$ that corresponds to the clockwise direction in the C_p - α curves, for upper surface pressure ports. Furthermore, for the pressure port located at $x/c=5\%$ of the upper surface, it is seen that for the higher oscillation amplitude cases, the separation phenomena is delayed up to the angle of attack of about 16.5 degrees for the pitching airfoil, and $\alpha=15.5$ degrees for the plunging one. Therefore it could be concluded that increasing the oscillation amplitude is more effective for the plunging motion than the pitching one because the pitch-rate in the pitching motion restrains the separation of the flow and decreases it.

4 Conclusions

Unsteady aerodynamic experiments were conducted on an oscillating airfoil in subsonic wind tunnel. The model was oscillated in two types of motions, pitch and plunge, at velocity of 30 m/sec, and a range of reduced frequencies, $k=0.029-0.1$. In addition, steady data were acquired and examined to furnish a baseline for analysis and comparison. The effect of reduced frequency and amplitude of motion was to increase the upper surface suction of the airfoil and resulted in higher variations of $|C_p|$ during one cycle oscillation. By oscillating the airfoil at higher mean angles of attack, the maximum suction increased also its location moved toward the leading edge. Also, pitch rate has strong influence in the data when oscillating the model in pitching near stall and post stall angles of attack.

5 Acknowledgment

The authors would like to thank the Iranian CERERA for the financial support of this project.

References

- [1] Leishman, J., Challenges in Modeling the Unsteady Aerodynamics of Wind Turbines, *presented at 21th ASME Wind Energy Symposium and the 40th AIAA Aerospace Sciences Meeting, Reno, 2002.*
- [2] Younsi, R., El-Batanong, I. Tritsch, J., Naji, H., and Landjerit, B., Dynamic Study of a Wind Turbine Blade with Horizontal Axis, *Sur. J. Mech. A/Solids* 20, 2001, pp. 241-252.
- [3] Huyer, S. A., Simms, D.A., and Robinson, M. C., Unsteady Aerodynamics Associated with a Horizontal-Axis Wind Turbines, *AIAA Journal*, Vol. 34, No. 7, 1997, pp. 1410-1419.
- [4] McCroskey, W.J., Recent Developments in Dynamic Stall, *Proc. of Unsteady Aerodynamics*, Vol. 1, p. 1, 1975.
- [5] McAlister, K. W., and Caw, L. W., Water Tunnel Visualization of Dynamic Stall, *Non steady Fluid Dynamics (ed. by Crow, P.E., and Miller, J. A.)*, p. 103, 1978.
- [6] Marseca, C., Favier, D., and Rebont, J., Experiments on an Airfoil at High Angle of Incidence in Longitudinal Oscillations, *Journal of Fluid Mechanics*, Vol. 92, 1979, pp. 671-690.
- [7] Broene, A. P., and Bragg, M. B., Spanwise Variation in the Unsteady Stalling Flowfields of Two-dimensional Airfoil Models, *AIAA Journal*, Vol. 39, No. 9, Sep. 2001, pp. 1641-1651.
- [8] Walker, J. M., Helin, H. E., and Chow, D. C., Unsteady Surface Pressure Measurement on a Pitching Airfoil, *AIAA Shear Flow Control Conference*, March 12-14, 1985.
- [9] S. A. Huyer, D.A. Simms, and M. C. Robinson, Unsteady Aerodynamics Associated with a Horizontal-Axis Wind Turbines, *AIAA Journal*, Vol. 34, No. 7, 1997, pp. 1410-1419.
- [10] M. C., Robinson, R. A. McD., Galbraith, D., Shipley, and M. Miller, Unsteady Aerodynamics of Wind Turbines, *Paper 95-0526, 33rd Aerospace Sciences Meeting, Reno, NV, Jan. 1995.*
- [11] Hansen, A. C., Butterfield, C. P., *Aerodynamics of Horizontal-Axis Wind Turbines*, Annu. Rev. Fluid Mech. 1993.
- [12] McCroskey W. J., Unsteady Airfoils, *Ann. Rev. Fluid Mech. U.S. Army Aerodynamics Laboratory and NASA*, 1982, pp. 285-309.
- [13] M.R. Soltani, F. Rasi, M. Seddighi, and A. Bakhshalipour, An Experimental Investigation of Time Lag in Pressure-Measuring Systems, *AIAC-2005-028, presented at 2nd Ankara International Aerospace Conference, Ankara, Turkey, Aug. 22-25, 2005.*
- [14] Carta, F., A Comparison of the Pitching and Plunging Response of an Oscillating Airfoil, *NASA CR-3172*, 1979.
- [15] Rae, H., William, Ir., Pope, Allan, *Low-Speed Wind Tunnel Testing*, 3rd Edition, John Wiley & Sons, 1999.

SURFACE PRESSURE VARIATION ON AN AIRFOIL IN PLUNGING AND PITCHING MOTIONS

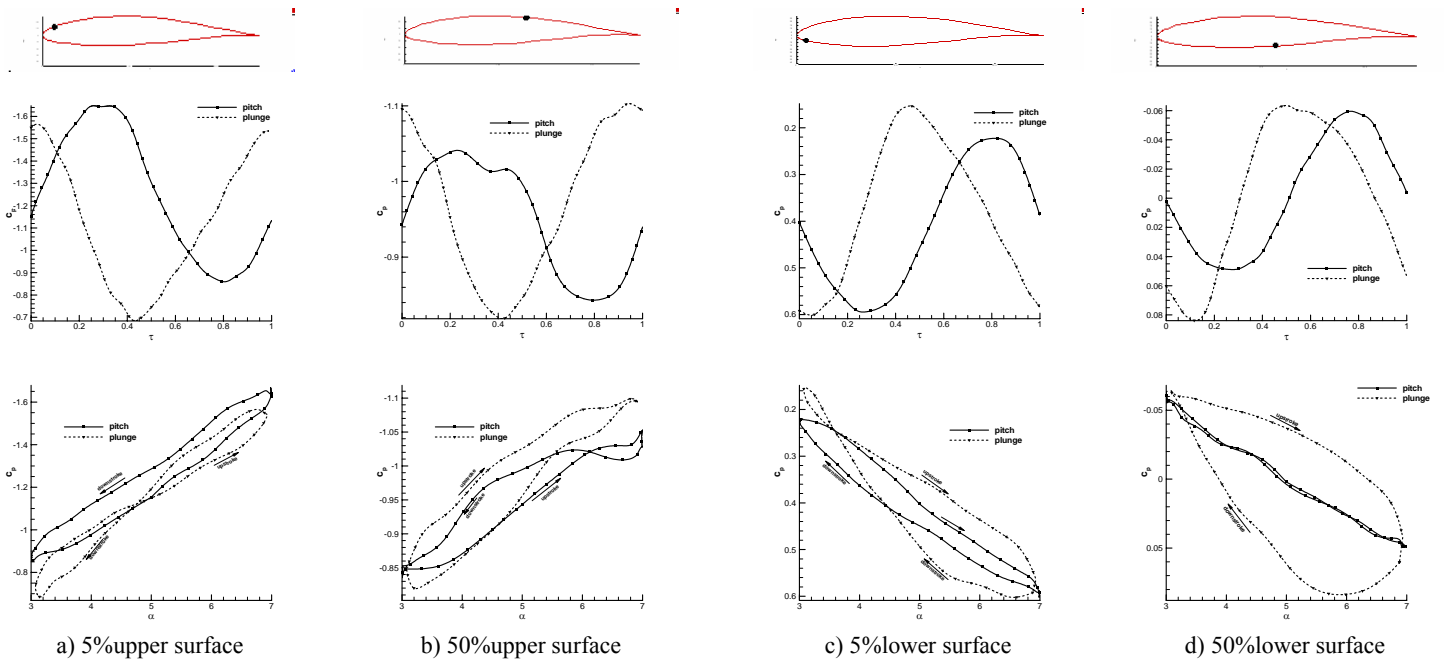


Fig. 4. Comparison of reduced frequency effects on the model pressure ports, $\alpha_0=5^\circ$, $\bar{\alpha}=2^\circ$, $V=30\text{m/s}$, $k=0.029$.

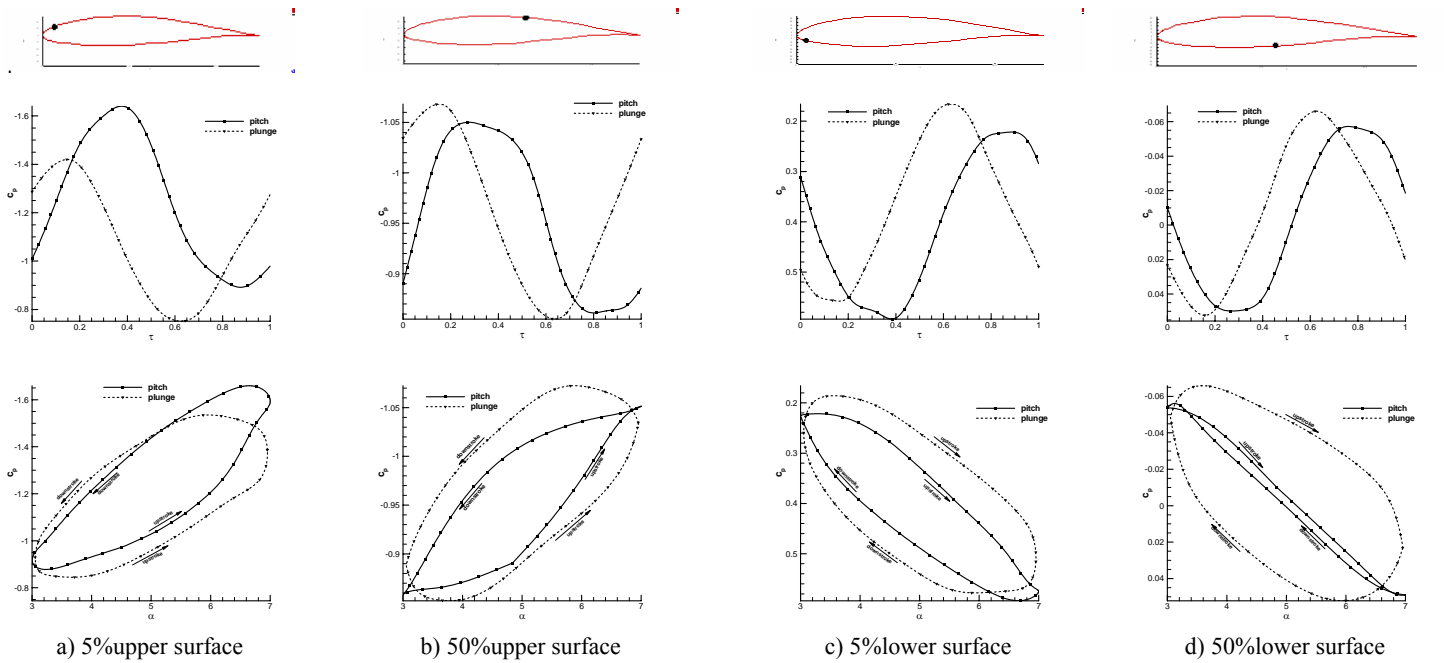


Fig. 5. Comparison of reduced frequency effects on the model pressure ports, $\alpha_0=5\text{deg}$, $\bar{\alpha}=2^\circ$, $V=30$, $k=0.087$.

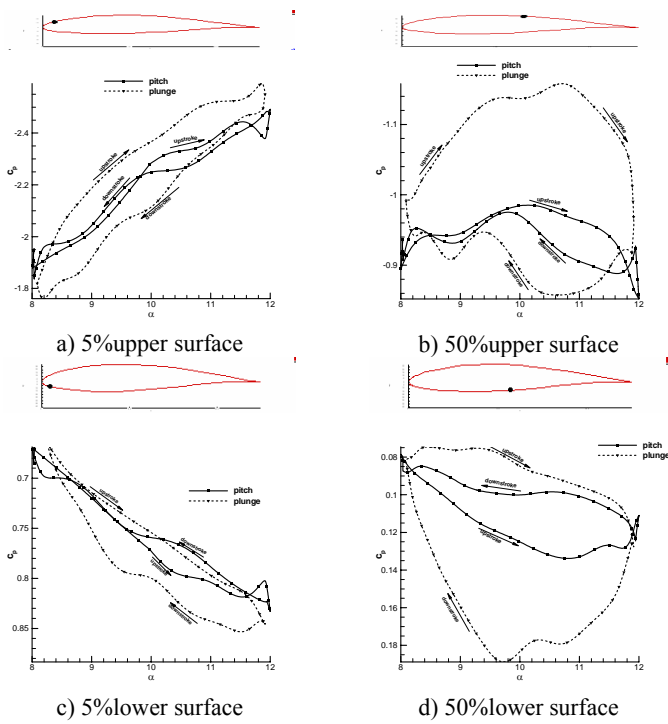


Fig. 6. Comparison of reduced frequency effects on the model pressure ports, $\alpha_0=10\text{deg}$, $\bar{\alpha}=2\text{deg}$, $V=30\text{m/s}$, $k=0.029$.

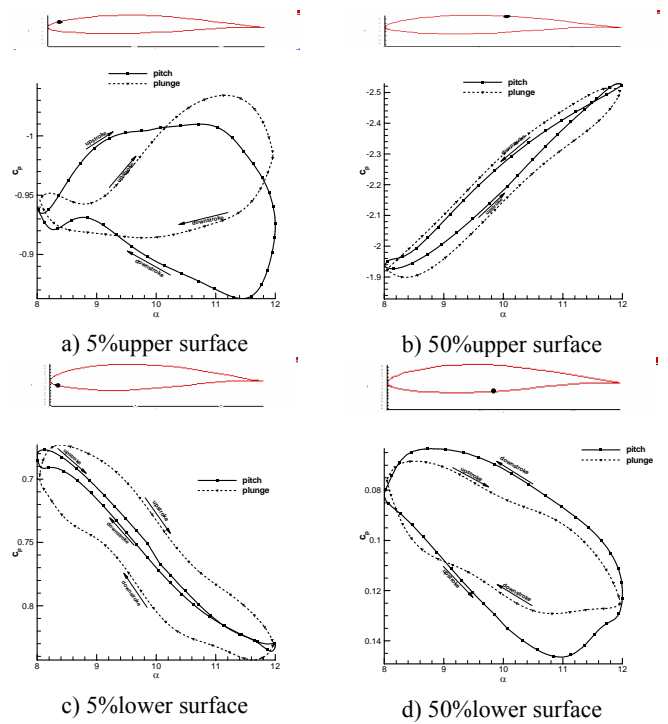


Fig. 7. Comparison of reduced frequency effects on the model pressure ports, $\alpha_0=10\text{deg}$, $\bar{\alpha}=2\text{deg}$, $V=30\text{m/s}$, $k=0.087$.

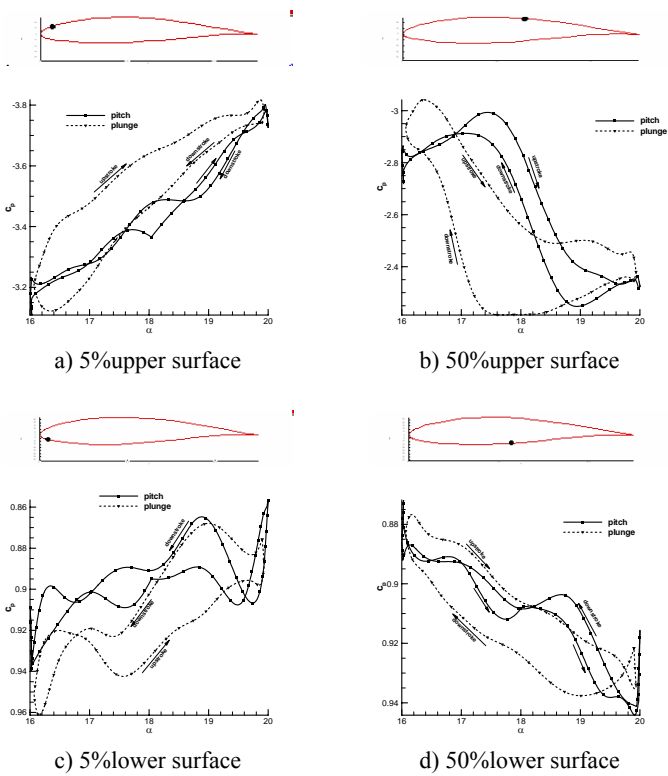


Fig. 8. Comparison of reduced frequency effects on the model pressure ports, $\alpha_0=18\text{deg}$, $\bar{\alpha}=2\text{deg}$, $V=30\text{m/s}$, $k=0.029$.

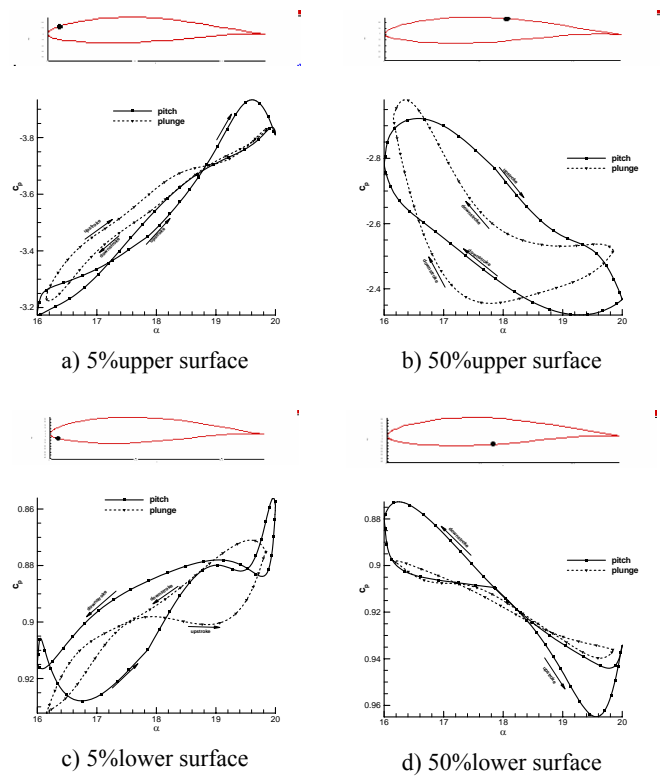


Fig. 9. Comparison of reduced frequency effects on the model pressure ports, $\alpha_0=18\text{deg}$, $\bar{\alpha}=2\text{deg}$, $V=30\text{m/s}$, $k=0.087$.

SURFACE PRESSURE VARIATION ON AN AIRFOIL IN PLUNGING AND PITCHING MOTIONS

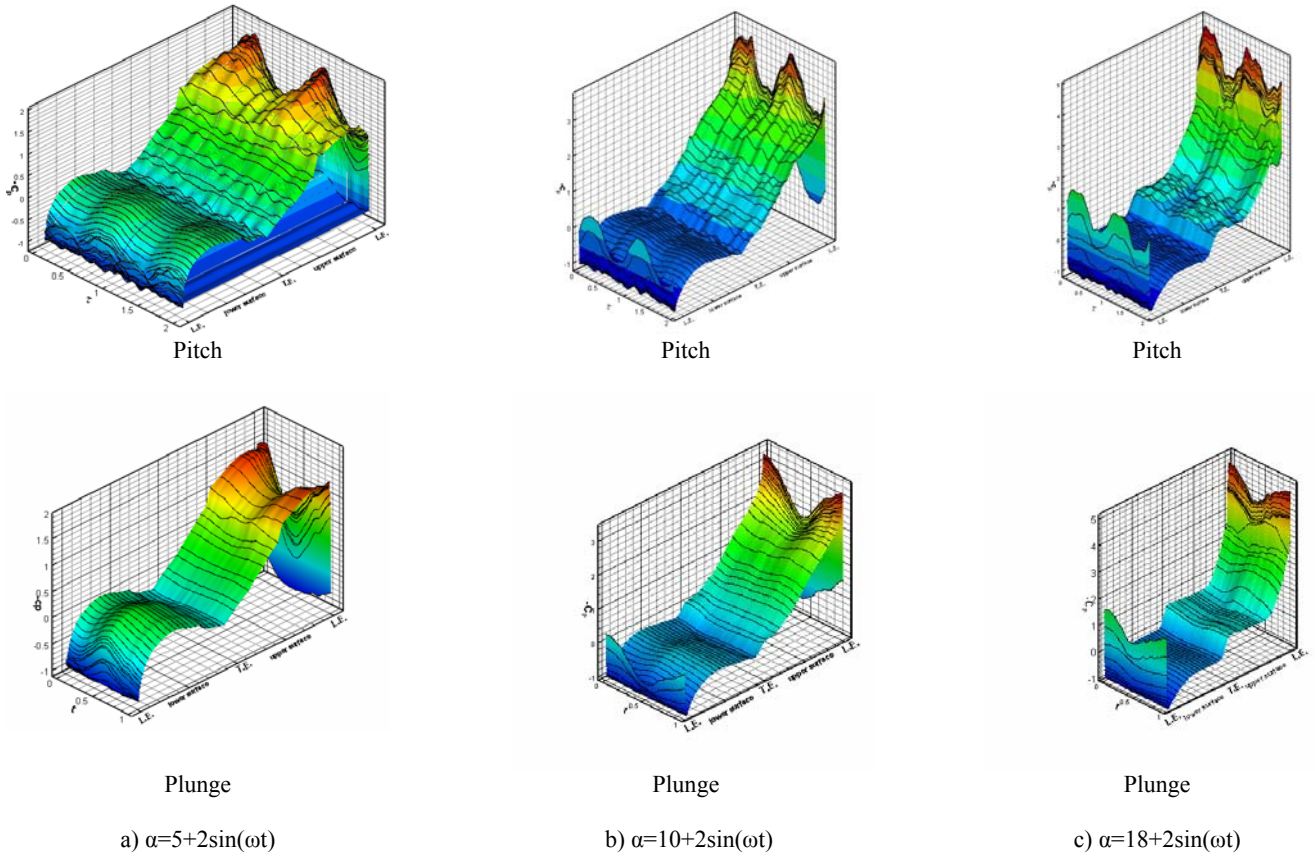


Fig. 10. Comparison of pitching and plunging surface pressure distributions

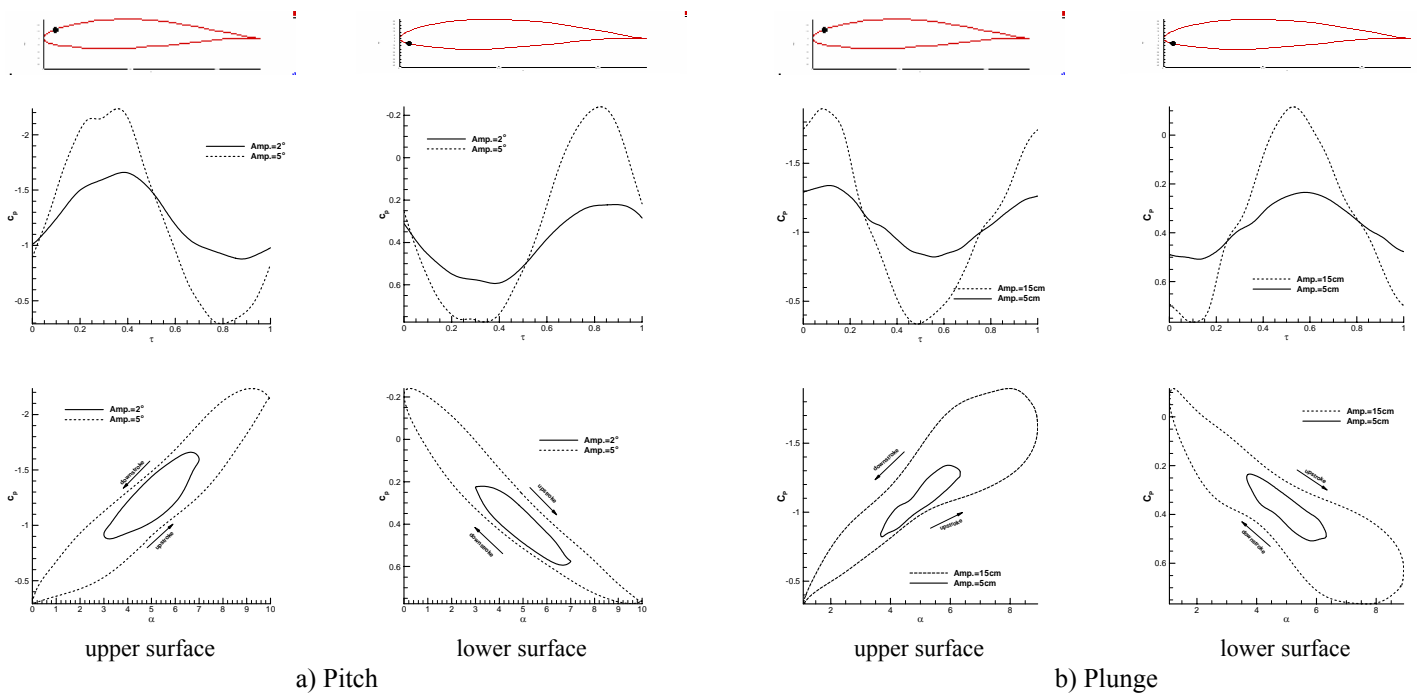


Fig. 11. Effect of amplitude of the motion, $\alpha_0=5$ deg, $k=0.058$, $V=30\text{m/s}$, $x/c=5\%$.

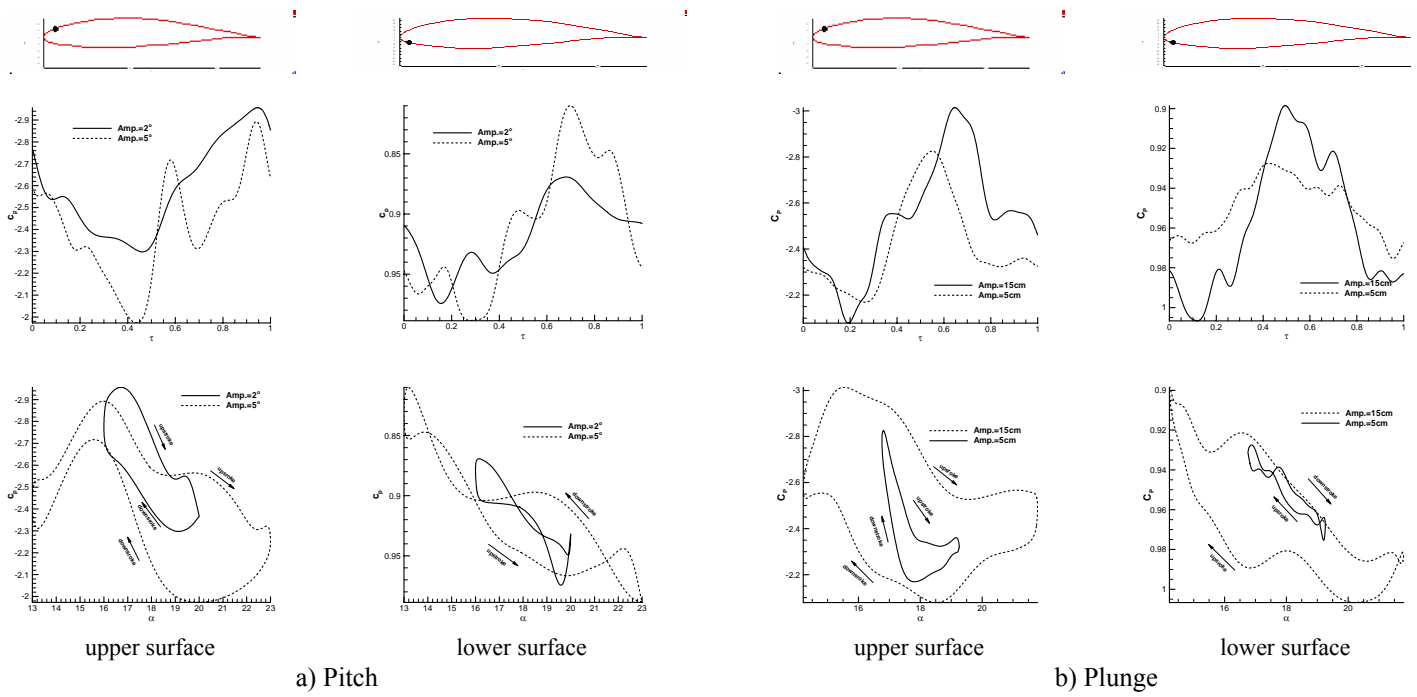


Fig. 12. Effect of amplitude of the motion, $\alpha_0=18$ deg, $k=0.058$, $V=30\text{m/s}$, $x/c=5\%$.